*Acta of Bioengineering and Biomechanics*
*Vol. 20, No. 4, 2018*

Original paper
DOI: 10.5277/ABB-01196-2018-02

# Modified Ginstling–Brounshtein model for wet precipitation synthesis of hydroxyapatite: analytical and experimental study

ANDREY E. KRAUKLIS[1, 2]*, IMANTS KREICBERGS[2], ILO DREYER[2]

[1] Department of Mechanical and Industrial Engineering, Norwegian University of Science and Technology, Trondheim, Norway.
[2] Institute of General Chemical Engineering, Riga Technical University, Riga, Latvia.

*Purpose:* Hydroxyapatite is the main mineral component in bones and teeth, thus being an important material in bone tissue engineering, e.g., for replacement and elimination of defects. Hydroxyapatite is widely used in real-life applications due to excellent biocompatibility and bioactivity. Wet precipitation synthesis of hydroxyapatite is limited by diffusivity. Hence, choice of a diffusion model becomes critical. The purpose of this work is three-fold. It experimentally validates the use of Ginstling–Brounshtein model for hydroxyapatite synthesis. It determines the effect of $Ca(OH)_2$ concentration on the kinetics and reports a modified model to account for this phenomenon. It reports obtained kinetic constants that describe hydroxyapatite synthesis. *Methods:* Particle size was determined using scanning electron microscopy and digital microscopy. Conversion kinetics were monitored using powder X-ray diffraction. *Results:* Experimental validation was provided. Furthermore, the process was found dependent on the calcium hydroxide concentration and the model was modified to account for this phenomenon. Kinetic constants describing the synthesis of hydroxyapatite were obtained and reported. *Conclusions:* The model was well consistent with the experimental data and can be used for describing synthesis of hydroxyapatite for various suspension concentrations.

*Key words*: *biomaterials, hydroxyapatite, synthesis, diffusion, Ginstling–Brounshtein model*

## List of symbols

HAp – Hydroxyapatite
WP – Wet precipitation
CaP – Calcium Phosphates
GB – Ginstling–Brounsthein
DI – Deionized
DGEBA – Bisphenol A diglycidyl ether
SEM – Scanning electron microscopy
XRD – X-ray diffraction
G – Conversion [–]
$K$ – Nominal kinetic constant [$m^2/s$]
$K_c$ – Concentration-independent kinetic coefficient [$m^2 \cdot M^{2/3}/s$]
$I$ – Integral intensity of a peak in a diffractogram [–]
$\tau$ – Time [s]
$R$ – Particle radius [m]
$S$ – Area of an agglomerate particle [$m^2$]
$K_\alpha$, $K_\beta$ – $K$-alpha and $K$-beta emission lines

# 1. Introduction

Hydroxyapatite (HAp) is the main mineral constituent of bones and teeth, and has found its application in various fields such as tissue engineering, orthopedics, prosthetics, drug transport and environmental remediation [7], [13], [14], [17]. During the recent decades, there have been various attempts in development and improvement of HAp synthetical methods, addressing novel scientific and economical aspects. Ideal synthetic HAp contains only such elements as Ca, P, O, H and furthermore Ca/P ratio has to be close to theoretical of 1.67 [23]. HAp is broadly used as a substrate material in tissue engineering**,** used in orthopedics, teeth implants and face surgery [7]. HAp is

* Corresponding author: Andrey E. Krauklis, Department of Mechanical and Industrial Engineering, Norwegian University of Science and Technology, 7491 Trondheim, Norway. Phone: +37126810288, e-mail: andrejs.krauklis@ntnu.no
Received: August 21st, 2018
Accepted for publication: August 24th, 2018

also used for chemical and biological purposes, such as chromatography, extraction of proteins and DNA, fractionation and purification of various biological molecules such as enzymes, nucleinic acids and antibody fragments [1], [17]. Recent studies have shown that HAp particles are able to inhibit growth of various cancer cells [8]. HAp is also used as a bioactive coating of metallic bone implants [20]. HAp and its derivatives are used in such, not connected to medicine, technologies as Michael type addition chemical reactions and oxidation of methane [25]. HAp is used in composite materials, for instance, in a bioactive $Al_2O_3$ and HAp composite. Such components possess high biocompatibility and are able to promote strong osteointegration within 3 months [18]. HAp is also used as a sorbent, for instance in sorption of $Pb^{2+}$; it has been reported that a HAp/$Fe_3O_4$ composite is able to sorb more than 99% $Pb^{2+}$ from solution [13].

Wet precipitation (WP) is one of the most widely used HAp synthesis methods and is based on the reaction of calcium hydroxide with the orthophosphoric acid diffusing into the particle. In the WP process, water solution of orthophosphoric acid is added dropwise to the aqueous suspension of calcium hydroxide [23]. The reaction can be written as in the Eq. (1).

$$10Ca(OH)_2 + 6H_3PO_4 \rightarrow Ca_{10}(PO_4)_6(OH)_2 + 18H_2O \quad (1)$$

WP synthesis is based on the fact that at room temperature at pH 4.2, HAp is least soluble and, as is often the case, also the most stable CaP (calcium phosphate) phase in aqueous solution [11], [22]. This method is widely studied and used in practice due to major advantages [23]: other elements are not involved in the reaction – only Ca, P, O, H are involved; the only side product in the main reaction is water. Other advantages of the precipitation method are that the method is clean as it involves non-polluting, somewhat simple and widely available compounds, and that there are possibilities for industrial application. The precipitation method has another advantage that it allows to control the powder morphology and the mean size, and it is a promising method for obtaining the nanosized HAp particles [17].

The typical procedure includes the dropwise addition of one reagent to the other, continuosly mixing, while keeping the molar ratio of elements Ca/P according to the stechiometry corresponding to HAp (Ca/P 1.67) [23]. As the last step, the obtained suspension should be stabilized at atmospheric pressure or can be washed right away, filtered, dried and ground into powder form [17].

Reaction is heterogeneous, it occurs mainly on the surface of calcium hydroxide particles, and to a lesser extent in the solution. Reaction in the solution occurs much less compared to the surface reaction, since the solubility of calcium hydroxide in water at room temperature and at atmospheric pressure is 0.17 g/100 mL [2], [19]. The effect of the concentration of $Ca(OH)_2$ suspension on the synthesis reaction is studied in this work.

The Ginstling–Brounshtein (GB) model is applicable for describing diffusion-controlled processes, and its practical use has been investigated and reported for a wide range of applications [5], [9], [10], [12], [15], [16], [21], [24]. Some of the applications that involve the GB model for describing the kinetics include solid-state synthesis reactions [16], dehydration of the iron(III) phosphate dihydrate [10], oxidation of carbon fibers and boron powder [5], [9], wollastonite fibre dissolution in acetic acid aqueous solution [15] and thermal degradation of DGEBA epoxy [21].

In this work, the diffusion model is analyzed in the context of diffusion of orthophosphoric acid into the calcium hydroxide particle in a water suspension. Since the chemical reaction is much faster than the diffusion, it can be assumed that the diffusion occurs into the reaction product (HAp) instead [6]. The model is somewhat simplified, since it does not account for the presence of byproducts which are normally created in the case of HAp synthesis [2].

Another important assumption is that particles can be considered as spherical, which is often only an approximation. In reality, $Ca(OH)_2$ particles are not ideally spherical. They are complicated agglomerates. However, such an assumption is necessary in order to get a convenient and practical model. The GB model is given by Eq. (2).

$$1-\frac{2}{3}G-(1-G)^{\frac{2}{3}}=\frac{K\tau}{R^2}, \quad (2)$$

where $G$ is conversion [–]; $K$ is nominal kinetic constant [$m^2/s$]; $\tau$ is time [s]; $R$ is particle radius [m].

The nominal kinetic constant $K$ is a parameter which describes diffusion and is related to the effective molecular diffusivity. When the value of $K$ is known, it becomes possible to predict the required time to achieve the desired conversion and design the synthesis accordingly.

Krauklis and Dreyer [12] have assessed the diffusion using the aforementioned GB model, using simulations and characteristic parameters for a laboratory-scale WP synthesis of HAp. It was deduced that the expected value of $K$ in the practical conditions of WP synthesis of HAp is $1.14\cdot10^{-17} \pm 4.33\cdot10^{-18}$ $m^2/s$ (95% probability).

The aim of this work is three-fold. First, it experimentally validates the use of GB model for the synthesis of HAp. Second aim is to determine the effect of $Ca(OH)_2$ concentration on the kinetics of the process and to modify the GB model accordingly to ac-

count for this phenomenon. Third aim is to obtain kinetic constants for describing the synthesis of HAp.

# 2. Materials and methods

HAp particles were prepared using the following method: calcium carbonate $CaCO_3$ from eggshells was calcinated at 1000 °C for an hour to obtain CaO. DI water was added to obtain the $Ca(OH)_2$ suspension of a desired concentration (0.15 and 0.30 M). This was followed by precipitation at 45 °C. While stirring, 2.00 M orthophosporic acid $H_3PO_4$ was added dropwise into the $Ca(OH)_2$ suspension. The rate of addition of $H_3PO_4$ solution was 6.8 mL/min. When the desired pH value was obtained, the suspension was stirred for an additional hour. The suspension was left for stabilization for 20 hours at room temperature and then filtered. The filtered precipitate was dried for 20 hours at 105 °C. The obtained powder was heated for 1 hour at 1100 °C.

All compounds used during this work were of analytical grade (≥98%). All aqueous solutions were prepared using high purity deionized water (10–15 MΩ·cm), produced via water purification system Millipore Elix 3 (Billerica, USA).

In the experimental part, in order to validate the model experimentally, particle size and conversion evolution in time should be determined. Furthermore, a suspension concentration dependence on process kinetics is studied and the modification of GB model is shown in order to account for this phenomenon.

## 2.1. Particle size determination

Scanning electron microscopy (SEM) was performed using Tescan Mira/LMU (Brno, Czech Republic) in backscattered electron regime with working voltage of 15 kV. Studied material was covered with a thin layer of gold in order to prevent charging due to electron beam. Gold sputtering was performed using Quorum Technologies Emitech K550X (Laughton, UK).

Optical microscopy was performed using a digital microscope Keyence VHX-2000 (Osaka, Japan) with a magnification of 5000×. Images for particle size analysis were processed using software NIH ImageJ (Bethesda, USA).

## 2.2. Conversion determination

X-ray diffraction (XRD) was performed using instrument Bruker D8 Advance (Billerica, USA). Radiation source: Cu $K_\alpha$, $\lambda$ = 1.54180 Å; Anode voltage 40 kV; Anode current 40 mA; $K_\beta$ filter 0.02 mm thick nickel foil; slits: divergence 0.6 mm, anti-scattering 8.0 mm; scanning range: $2\theta$ = 3 – 55°, step 0.02°, step time 0.5 s; energy-dispersive one-dimensional detector Lynx Eye.

Conversion determination procedure had complications. During the reaction, samples have to be analyzed for $Ca(OH)_2$ content. In order to do so, the reaction has to be stopped. The conversion data was obtained after a rapid cooling of samples in liquid nitrogen. However, also in such conditions calcium hydroxide carbonization might occur and should be monitored. Furthermore, in the end of the process, when part of hydroxide had reacted, peaks became hard to detect.

# 3. Results

## 3.1. Particle size determination

Based on SEM micrographs, shown in Fig. 1, the size of $Ca(OH)_2$ particles is in the range of 1–3 μm, or the radius is 0.5–1.5 μm.

SEM micrographs did not represent the real size of the agglomerates, because SEM cannot be used in solutions and suspensions. Nevertheless, particle size values obtained with SEM show that the size could be determined using digital microscopy of a $Ca(OH)_2$ suspension. It can be seen in Fig. 1 (right), that nanoparticle agglomerates were obtained, as expected based on literature [2].

Calcium hydroxide suspension used for WP synthesis of HAp is shown in Fig. 2. On the left, the raw micrograph of the suspension obtained with the optical microscope is shown. On the right, the micrograph after noise removal is shown, indicating measured particles in black colour. Spherical particle size can be undoubtedly well represented by a diameter. However, if the object is not ideally spherical, real particle size can be substituted with a hypothetical one, which shares some identical qualities. In this case, the area can be considered an identical parameter. When the area is known, agglomerate equivalent radii $R$ can be calculated as shown in Eq. (3).

$$R = \sqrt{\frac{S}{\pi}}, \tag{3}$$

where $S$ is area of an agglomerate particle. 198 agglomerate particles were measured (marked in black

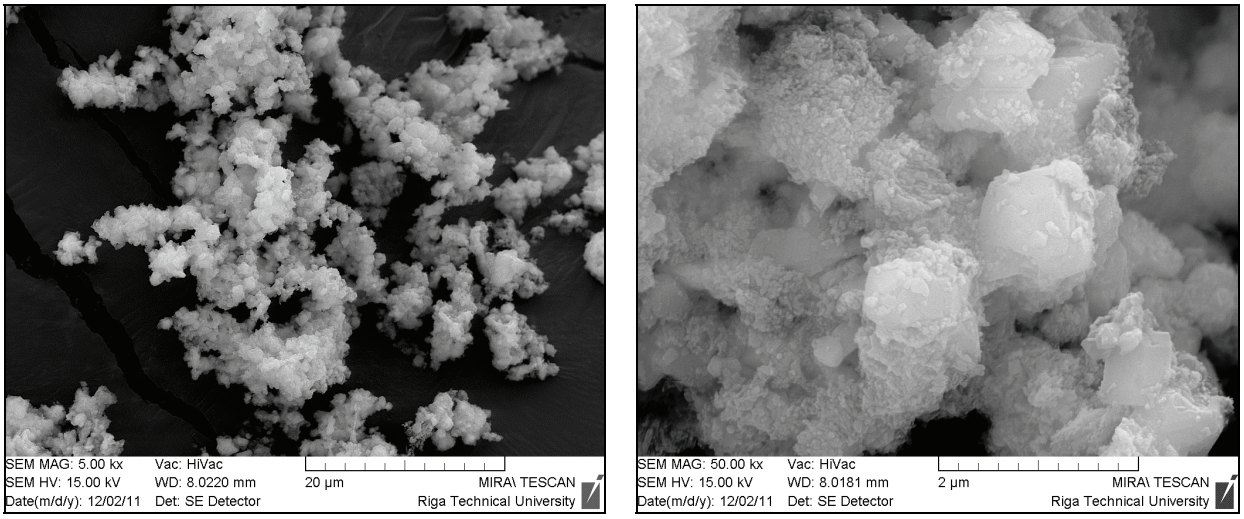


Fig. 1. SEM micrographs of $Ca(OH)_2$ used for particle size determination

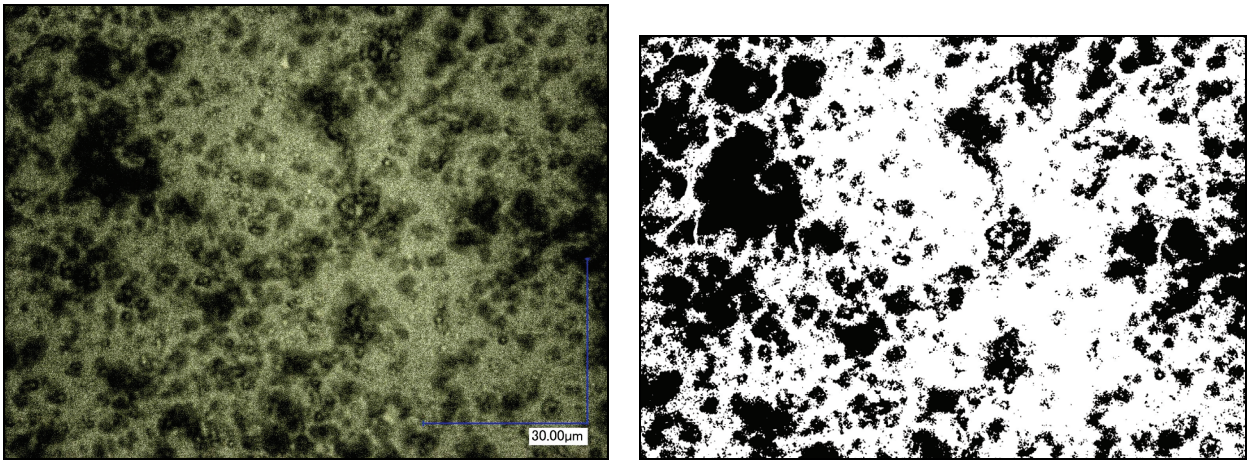


Fig. 2. Calcium hydroxide suspension after the ball mill; left: view in a digital microscope;
right: after noise removal as used for particle size analysis (particles used for analysis are marked in black)

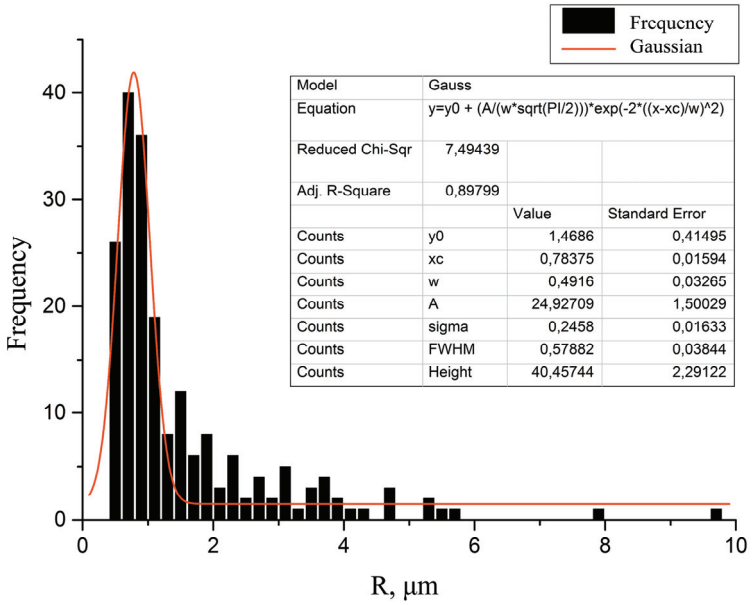


Fig. 3. Particle size distribution

in Fig. 2: right), and the equivalent radii were obtained from the area of the particles by using the Eq. (3). The equivalent radii were in the range from 0.5 to 9.7 μm. Particle size distribution is shown in Fig. 3. An average agglomerate size is equal to $x_c \pm 2\sigma = 0.78375 \pm 0.4916$ μm (95% probability). Furthermore, particle size distribution is well represented by a normal distribution (Gaussian, Fig. 3). The determination coefficient is equal to $R^2 = 0.90$, showing a fairly good fit of experimental data with a normal distribution. The fitting curve is skewed to the right, which is believed to be due to approaching the detection limit of the microscope (about 0.5 μm).

## 3.2. Conversion determination

Using XRD analyses, evolution of integral intensities of $Ca(OH)_2$ and HAp peaks was studied in time,

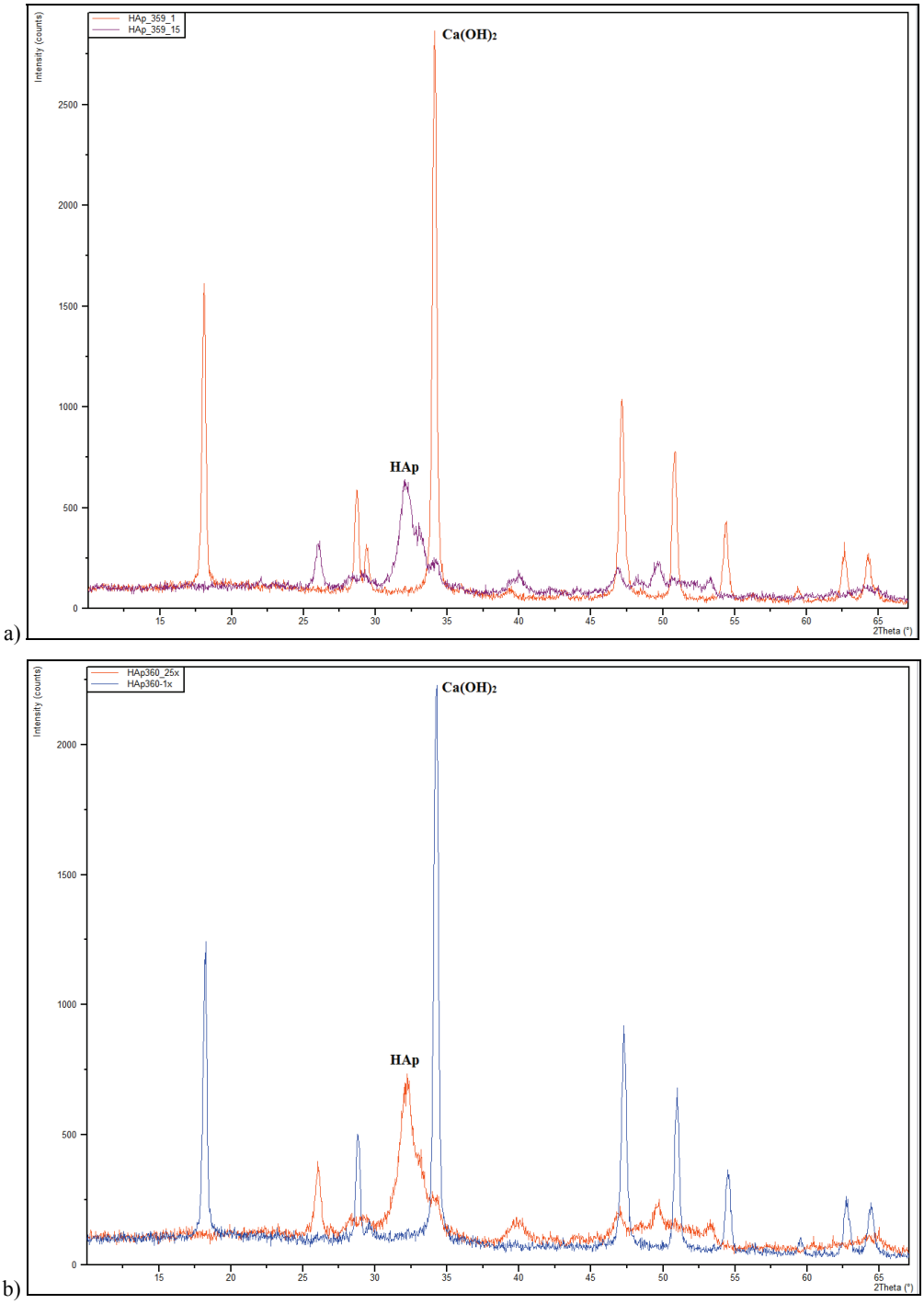


Fig. 4. First and last diffractograms of (a) 0.15 M $Ca(OH)_2$ suspension and (b) 0.30 M $Ca(OH)_2$ suspension

providing information on conversion kinetics. Two suspensions were studied:

- 0.15 M $Ca(OH)_2$ suspension; 2.00 M $H_3PO_4$ with addition rate of 6.8 mL/min.
- 0.30 M $Ca(OH)_2$ suspension; 2.00 M $H_3PO_4$ with addition rate of 6.8 mL/min.

Most intensive peaks of HAp and $Ca(OH)_2$ were used for the analysis, since influence of noise on them is least prominent. Noise levels were about 40 in intensity, thus intentisties that had values lower than this value were impossible to detect. These peaks were chosen based on literature [3], [4]. XRD diffractograms are shown in Fig. 4.

XRD analysis results for 0.15 M and 0.30 M $Ca(OH)_2$ suspensions are shown in Tables 1 and 2, respectively.

Table 1. 0.15 M $Ca(OH)_2$ suspension XRD data

| Time $\tau$ [min] | Integral intensity HAp | Integral intensity $Ca(OH)_2$ |
|---|---|---|
| 1 | 53.8 | 2690.4 |
| 3 | 144.3 | 1906.9 |
| 5 | 251.2 | 1639.8 |
| 7 | 355.0 | 1343.0 |
| 11 | 534.3 | 381.5 |
| 13 | 612.8 | 199.5 |
| 15 | 541.2 | 144.9 |

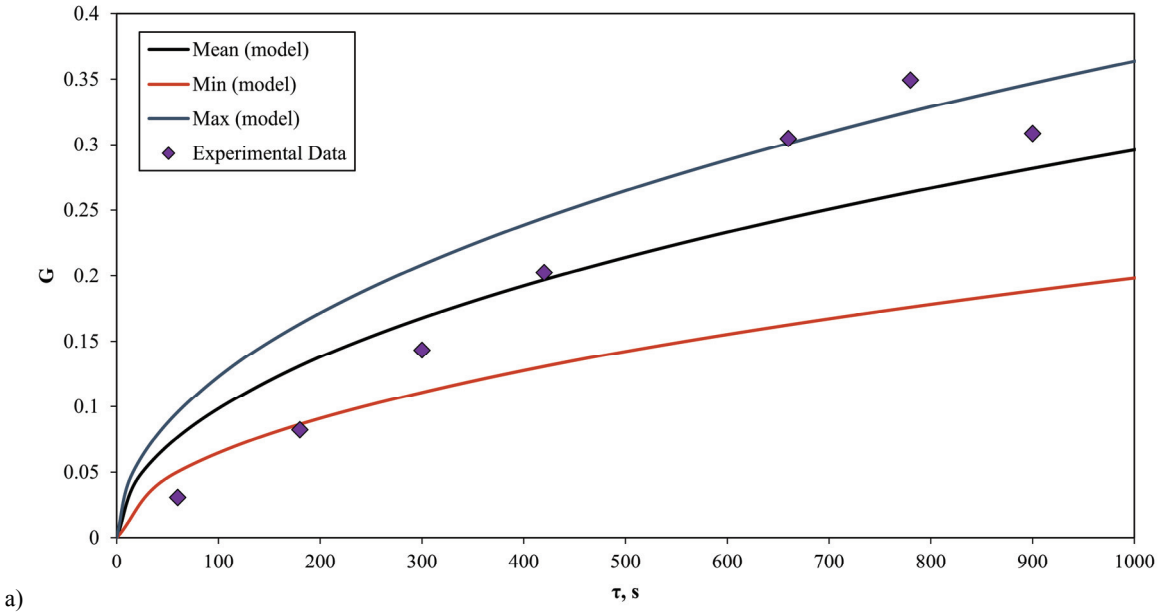


a)

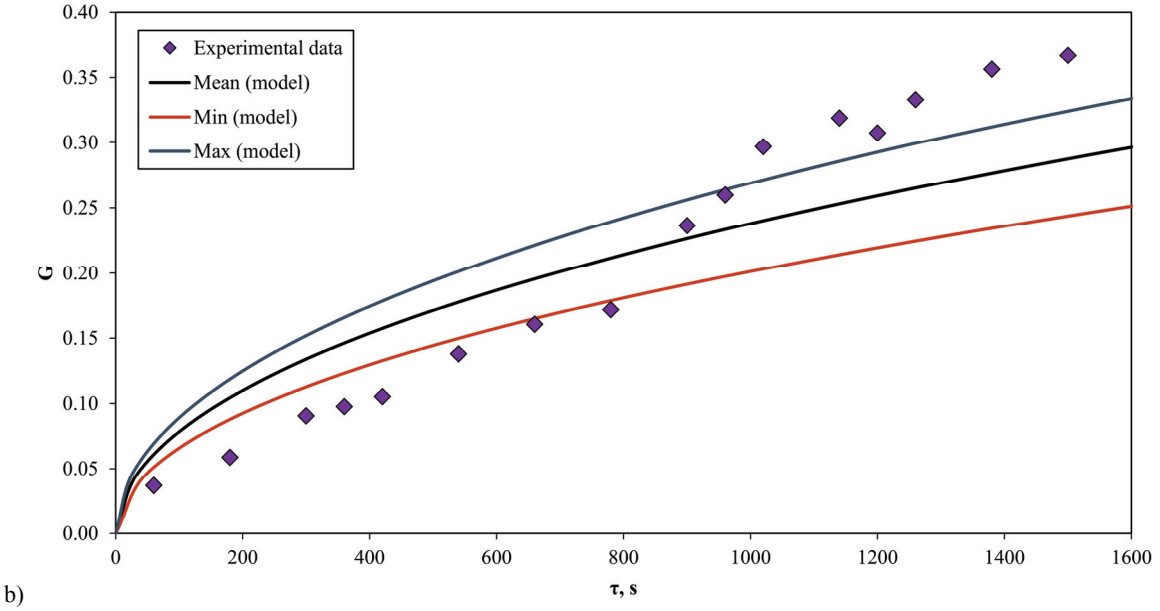


b)

Fig. 5. Experimentally determined conversion in time and GB model using minimum, average and maximum values for a kinetic constant for: (a) 0.15 M $Ca(OH)_2$ suspension, (b) 0.30 M $Ca(OH)_2$ suspension

Table 2. 0.30 M $Ca(OH)_2$ suspension XRD data

| Time $\tau$ [min] | Integral intensity HAp | Integral intensity $Ca(OH)_2$ |
|---|---|---|
| 1 | 63.7 | 2136.3 |
| 3 | 101.5 | 1989.1 |
| 5 | 156.4 | 2164.0 |
| 6 | 168.6 | 1777.5 |
| 7 | 181.7 | 1369.2 |
| 9 | 238.1 | 1469.9 |
| 11 | 277.2 | 1339.8 |
| 13 | 296.5 | 924.9 |
| 15 | 408.1 | 809.0 |
| 16 | 448.4 | 711.1 |
| 17 | 512.4 | 523.8 |
| 19 | 550.6 | 435.5 |
| 20 | 530.8 | 354.1 |
| 21 | 575.0 | 213.8 |
| 23 | 615.2 | 202.7 |
| 25 | 633.6 | 202.5 |

XRD analysis of products after thermal treatment shows that the integral intensity of a HAp peak $I_{\max_{HAp}}$ is 1754.2 and 1726.1 in the case of 0.15 M and 0.30 M $Ca(OH)_2$ suspension, respectively. It is assumed that in each case this corresponds to a full conversion ($G = 1$). The conversion at each time step can be calculated using Eq. (4).

$$G(\tau) = \frac{I(\tau)_{HAp}}{I_{\max_{HAp}}} \tag{4}$$

where $I(\tau)_{HAp}$ is integral intensity of HAp peak after a known time.

Experimentally obtained conversion evolution in time is shown in Fig. 5.

## 3.3. $K/R^2$ ratio determination: analysis via descriptive statistics, *F*-test and *t*-test

When the conversion and the time it took to reach it are known, it is possible to obtain $K/R^2$ ratio for both 0.15 M and 0.30 M $Ca(OH)_2$ suspension case by introducing $G$ and $\tau$ data into the GB equation.

$$1 - \frac{2}{3}G - (1-G)^{\frac{2}{3}} = \frac{K\tau}{R^2} \tag{5}$$

$K/R^2$ ratios obtained this way are $1.1273 \cdot 10^{-5} \pm 6.4719 \cdot 10^{-6}$ $s^{-1}$ and $7.0699 \cdot 10^{-6} \pm 2.1120 \cdot 10^{-6}$ $s^{-1}$ for 0.15 M and 0.30 M $Ca(OH)_2$ suspension, respectively (probability 95%).

Using the obtained data and the model, six simulations were performed: three per suspension – using the minimum, average and maximum $K/R^2$ ratio (95% probability) for each case (0.15 M and 0.30 M $Ca(OH)_2$ suspension). The results of the simulation runs are shown in Fig. 5 in the $G - \tau$ coordinates. Purple data points represent the experimental data. Red, black and blue lines represent the model with minimum, average and maximum $K/R^2$ ratio used, respectively.

The difference between $K/R^2$ ratio average values for 0.15 M and 0.30 M $Ca(OH)_2$ suspension was 37.28%. In order to determine whether results can be considered identical or significantly different, *t*-test is performed.

The results of *F*-test are summarized in Table 3. Fisher critertion ($\alpha = 0.05$) is $F = 3.117$, *p*-value was 0.0346, and the critical value of Fisher criterion was 2.790. Dispersions of two suspensions' data sets differ significantly (96.54% probability) since Fisher criterion ($\alpha = 0.05$) $F = 3.117 > F_{0.05} = 2.790$ and $P(F \leq f)_{\text{one-tail}} = 0.0346 < 0.05$. This shows that the uncertainty within both experiments vary.

Table 3. *F*-test results

| Statistics | 0.15 M $Ca(OH)_2$ suspension: $K/R^2$ | 0.30 M $Ca(OH)_2$ suspension: $K/R^2$ |
|---|---|---|
| Mean value | $1.13 \cdot 10^{-5}$ | $7.07 \cdot 10^{-6}$ |
| Dispersion | $4.9 \cdot 10^{-11}$ | $1.57 \cdot 10^{-11}$ |
| Observations | 7 | 16 |
| Degrees of freedom | 6 | 15 |
| Fisher criterion | 3.117 | |
| *p*-value (one-tail) | 0.0346 | |
| Fisher criterion's critical value | 2.790 | |

Since dispersions vary, then the *t*-test with two-sample assuming unequal variances was used to compare $K/R^2$ mean values of 0.15 M and 0.30 M $Ca(OH)_2$

Table 4. *t*-test results

| Statistics | 0.15 M $Ca(OH)_2$ suspension: $K/R^2$ | 0.30 M $Ca(OH)_2$ suspension: $K/R^2$ |
|---|---|---|
| Mean value | $1.13 \cdot 10^{-5}$ | $7.07 \cdot 10^{-6}$ |
| Dispersions | $4.9 \cdot 10^{-11}$ | $1.57 \cdot 10^{-11}$ |
| Observations | 7 | 16 |
| Null hypothesis ($H_0$: $\bar{x} = \bar{y}$) | 0 | |
| Degrees of freedom | 8 | |
| Factual *t*-value ($t_{\text{Stat}}$) | 1.488 | |
| *p*-value (one-tail) | 0.0875 | |
| Critical *t*-value (one-tail) ($\alpha = 0.05$) | 1.860 | |
| Critical *t*-value (one-tail) ($\alpha = 0.088$) | 1.484 | |

suspensions in order to determine if the difference between them is statistically significant. The null hypothesis then is ($H_0$: $\bar{x} = \bar{y}$)) that both values do not differ significantly. The null hypothesis is checked using *t*-test and results are shown in Table 4.

Factual *t*-value was 1.488, critical *t*-value was 1.860 ($\alpha$ = 0.05) and 1.484 ($\alpha$ = 0.088). In order to disprove the null hypothesis, factual *t*-value has to be larger than the critical one, besides *p*-value has to be lower than $\alpha$.

With 95% probability, null hypothesis ($H_0$) is not disproved based on *t*-value at $\alpha$ = 0.05. However, with only slightly lower probability of 91.2%, null hypothesis is disproved ($\alpha$ = 0.088), and in both sample collections (0.15 M and 0.30 M $Ca(OH)_2$ suspensions) mean values are significantly different, since $t_{Stat}$ = 1.488 > $t_{Critical\ one\text{-}tail}$ = 1.484, also $P(T \leq t)_{one\text{-}tail}$ = 0.0875 < 0.0880.

Since $K/R^2$ values for 0.15 M and 0.30 M $Ca(OH)_2$ suspension data differ significantly at $\alpha$ = 0.088, it means that with a 91.2% probability suspension concentration has an effect on the kinetics of the process. This is also due to the fact that concentration of the suspension is the only parameter that differs between experimental data series of 0.15 M and 0.30 M $Ca(OH)_2$ suspensions.

## 3.4. $K/R^2$ ratio determination: regression analysis

Value range of $K/R^2$ ratios was broad, hence another method – regression analysis – was used. The model

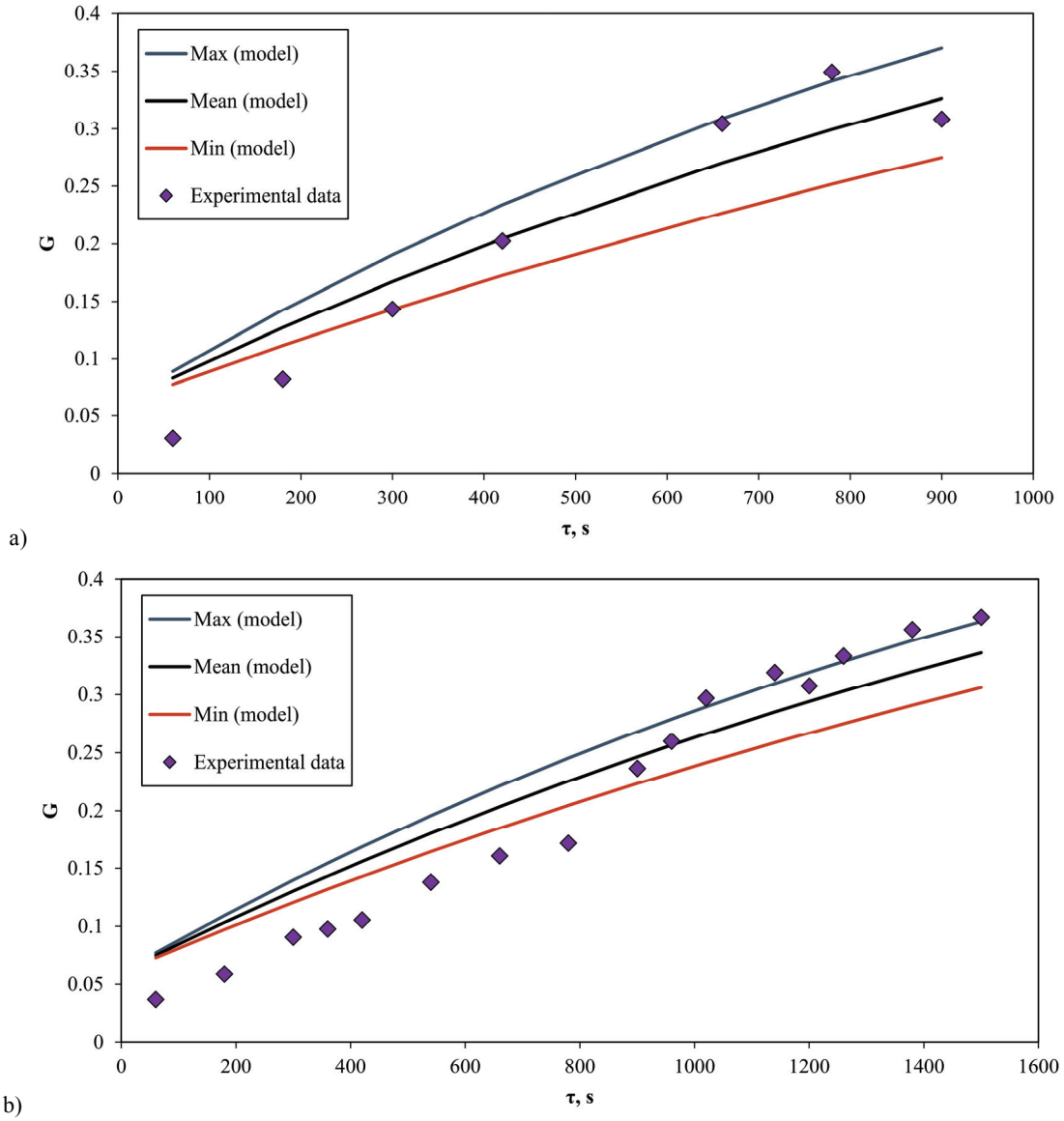


Fig. 6. Conversion evolution in time obtained using regression analysis of experimental data of: (a) 0.15 M $Ca(OH)_2$ suspension and (b) 0.30 M $Ca(OH)_2$ suspension series

is not linear and data cannot be linearized. In order to use the linear regression, it is necessary to transform the GB equation into Eq. (5).

$$Z = \frac{K\tau}{R^2}, \tag{5}$$

where

$$Z = 1 - \frac{2}{3}G - (1-G)^{\frac{2}{3}} \tag{6}$$

$Z$ values are calculated, the results of regression analysis are shown in Fig. 6a.

Using regression analysis, the mean value of $K/R^2$ was determined to be $1.61 \cdot 10^{-5}$ $s^{-1}$ for 0.15 M $Ca(OH)_2$ suspension. Determination coefficient is 0.943. With a 95% probability the value of $K/R^2$ ratio is in the range from $1.21 \cdot 10^{-5}$ to $2.01 \cdot 10^{-5}$ $s^{-1}$, which is 24.84% uncertainity in each direction.

The mean value of $K/R^2$ is determined to be $1.02 \cdot 10^{-5}$ $s^{-1}$ for 0.30 M $Ca(OH)_2$ suspension. Determination coefficient is 0.934. With a 95% probability the value of $K/R^2$ ratio is in the range from $8.67 \cdot 10^{-6}$ to $1.16 \cdot 10^{-5}$ $s^{-1}$, which is 14.63% uncertainity in each direction.

Figure 6 shows the conversion evolution in time, and that the dispersion of $K/R^2$ results, both in the case of 0.15 M and 0.30 M $Ca(OH)_2$ suspension, which were obtained using regression analysis with a 95% probability, is smaller than the dispersion in results obtained from descriptive statistics (shown in Fig. 5).

## 3.5. Kinetic constant determination

It is now possible to calculate the kinetic constant $K$ by multiplying the obtained $K/R^2$ ratio and the square of a measured particle size. Minimum, mean and maximum (95% probability) obtained $K/R^2$ ratio, $R$ and $K$ values are systematized and reported in Table 5 for both 0.15 M and 0.30 M $Ca(OH)_2$ suspensions.

Table 5. Obtained $K/R^2$ ratio, $R$ and $K$ values

| 0.15 M $Ca(OH)_2$ suspension | | | |
|---|---|---|---|
| | Min | Mean | Max |
| $R$ [m] | $2.9 \cdot 10^{-7}$ | $7.8 \cdot 10^{-7}$ | $1.28 \cdot 10^{-6}$ |
| $K/R^2$ [$s^{-1}$] (descriptive) | $4.80 \cdot 10^{-6}$ | $1.13 \cdot 10^{-5}$ | $1.77 \cdot 10^{-5}$ |
| $K/R^2$ [$s^{-1}$] (regression) | $1.21 \cdot 10^{-5}$ | $1.61 \cdot 10^{-5}$ | $2.01 \cdot 10^{-5}$ |
| $K$ [$m^2/s$] (descriptive) | $4.04 \cdot 10^{-19}$ | $6.86 \cdot 10^{-18}$ | $2.91 \cdot 10^{-17}$ |
| $K$ [$m^2/s$] (regression) | $1.02 \cdot 10^{-18}$ | $9.80 \cdot 10^{-18}$ | $3.29 \cdot 10^{-17}$ |
| 0.30 M $Ca(OH)_2$ suspension | | | |
| | Min | Mean | Max |
| $R$ [m] | $2.9 \cdot 10^{-7}$ | $7.8 \cdot 10^{-7}$ | $1.28 \cdot 10^{-6}$ |
| $K/R^2$ [$s^{-1}$] (descriptive) | $4.96 \cdot 10^{-6}$ | $7.07 \cdot 10^{-6}$ | $9.18 \cdot 10^{-6}$ |
| $K/R^2$ [$s^{-1}$] (regression) | $8.67 \cdot 10^{-6}$ | $1.02 \cdot 10^{-5}$ | $1.16 \cdot 10^{-5}$ |
| $K$ [$m^2/s$] (descriptive) | $4.17 \cdot 10^{-19}$ | $4.30 \cdot 10^{-18}$ | $1.50 \cdot 10^{-17}$ |
| $K$ [$m^2/s$] (regression) | $7.29 \cdot 10^{-19}$ | $6.21 \cdot 10^{-18}$ | $1.90 \cdot 10^{-17}$ |

## 3.6. Modification of the GB model: introducing concentration dependence

As mentioned before, $K/R^2$ values for cases of 0.15 M and 0.30 M $Ca(OH)_2$ suspensions are significantly different (91.2% probability), thus it can be stated that suspension concentration has an effect of process kinetics, since it is the only parameter that differs between the experimental series.

Since there is the same amount of acid introduced, but the amount of $Ca(OH)_2$ is larger, then the reaction time should also increase. This hypothesis will now be evaluated using the obtained $K$ values for 0.15 M and 0.30 M $Ca(OH)_2$ suspensions. The hypothesis is the following: if $K$ value is dependent on suspension concentration, then the GB model can be modified, and if the relationship between conversion and suspension concentration is found, it is possible to obtain a suspension concentration-independent kinetic constant $K_c$. Then the following is valid:

$$K = K_c \cdot C_{\mathrm{Ca(OH)_2}}^{x} \tag{7}$$

Since the only parameter that differs is the concentration of suspension and $K_c$ being independent of suspension concentration, it is possible to write the following:

$$K_c = \frac{K_{0.15M}}{0.15^x} = \frac{K_{0.30M}}{0.30^x}, \tag{8}$$

$$x = \log_2 \frac{K_{0.30M}}{K_{0.15M}}, \tag{9}$$

where $K_{0.15M}$ and $K_{0.30M}$ are kinetic constants in case of 0.15 M and 0.30 M suspensions, respectively. Using obtained mean values of $K$ from the regression analysis data of $K/R^2$:

$$x = \log_2 \frac{6.21 \cdot 10^{-1\mathrm{s}}}{9.80 \cdot 10^{-1\mathrm{s}}} = -0.658 \tag{10}$$

Using obtained mean values of $K$ from the descriptive statistics data of $K/R^2$:

$$x = \log_2 \frac{4.30 \cdot 10^{-18}}{6.86 \cdot 10^{-18}} = -0.673 \tag{11}$$

On average, $x$ is –0.667. The concentration-independent $K_c$ becomes then:

$$K_c = K \cdot C_{Ca(OH)_2}^{-x} = K \cdot C_{Ca(OH)_2}^{\frac{2}{3}} \quad (12)$$

Inserting the obtained values for 0.15 M and 0.30 M $Ca(OH)_2$ suspensions using regression analysis and descriptive statistics $K/R^2$ values, respectively, the mean $K_c$ value for synthesis of HAp are $2.77 \cdot 10^{-18}$ $m^2 \cdot M^{2/3}/s$ and $1.93 \cdot 10^{-18}$ $m^2 \cdot M^{2/3}/s$.

The modified GB equation that accounts for suspension concentration for the synthesis of HAp is obtained (Eq. (13)):

$$1 - \frac{2}{3}G - (1-G)^{\frac{2}{3}} = \frac{K_c \tau}{R^2 C_{Ca(OH)_2}^{\frac{2}{3}}} \quad (13)$$

The modified GB model shows that the higher the suspension concentration, the longer time is necessary to obtain the same conversion if all other parameters are unchanged.

# 4. Discussion

Mean values of kinetic constants $K$ for 0.15 M and 0.30 M $Ca(OH)_2$ suspensions obtained using regression analysis $K/R^2$ values are $9.80 \cdot 10^{-18}$ and $6.21 \cdot 10^{-18}$ $m^2/s$, respectively. Mean values of $K$ for 0.15 M and 0.30 M $Ca(OH)_2$ suspensions, calculated using descriptive statistics $K/R^2$ values, are $6.86 \cdot 10^{-18}$ and $4.30 \cdot 10^{-18}$ $m^2/s$, respectively. Taking the statistical uncertainties into account, these results are considered identical.

The conversion evolution with time $G = f(\tau)$ relationship for HAp synthesis was found with a good agreement with the experimental data, however a range of possible $K$ values with a 95% probability is broad. It can be seen that uncertainties are large, especially possible maximum values of $K$ (maximum uncertainty reaches 236.20%), which is due to calculation procedure of $K$ using $R$ squared, which introduces then uncertainty of particle size determinations squared.

Experimentally, average agglomerate size was found to be 0.78 μm, but the standard deviation was fairly high (0.25 μm), meaning that particles were not very uniform in size. Particle size distribution was fairly well represented by a normal distribution (determination coefficient $R^2 = 0.90$). The method using optical microscopy of a suspension was sufficient to determine particle size and draw the conclusions, however, the authors believe that other methods of particle size determination should also be considered for a more careful approach, especially when smaller particle size is of interest. This is due to the fact that the largest uncertainty is introduced by particle size determination.

The range of $K/R^2$ ratio values obtained from the regression analysis is considered a better result than from descriptive statistics due to a smaller uncertainty and an average $R$ value.

# 5. Conclusions

In the previous study, a statistical and mathematical analysis of Ginstling–Brounshtein (GB) model showed that it can be used to describe a wet precipitation (WP) synthesis of hydroxyapatite (HAp). Based on the experimental evidence in this work the following conclusions were made:

1. Statistical and mathematical analysis of GB model showed that it can be used in the case of HAp.
2. As a result of mathematical simulations, a range of possible $K$ values (95% probability) in the synthesis was obtained in previous work ($1.143 \cdot 10^{-17} \pm 4.330 \cdot 10^{-18}$ $m^2/s$) and was found consistent with the experimental data reported in this work.
3. The model is well consistent with the experimental data. Obtained $K/R^2$ ratio (95% probability) in the case of 0.15 M and 0.30 M $Ca(OH)_2$ is $1.61 \cdot 10^{-5} \pm 0.40 \cdot 10^{-5}$ $s^{-1}$ and $1.02 \cdot 10^{-5} \pm 1.49 \cdot 10^{-6}$ $s^{-1}$, respectively. As a result of regression analysis, $G = f(\tau)$ graphs were made for both 0.15 M and 0.30 M $Ca(OH)_2$, showing time required to achieve a specific rate of conversion.
4. Obtained $K$ values in the case of 0.15 M and 0.30 M $Ca(OH)_2$ are $9.8 \cdot 10^{-18} \pm 2.4 \cdot 10^{-18}$ $m^2/s$ and $6.2 \cdot 10^{-18} \pm 9.0 \cdot 10^{-19}$ $m^2/s$ (using the average $R$ value), respectively. Taking $R$ uncertainty into account, $K$ value is in range from $1.02 \cdot 10^{-18}$ to $3.29 \cdot 10^{-17}$ $m^2/s$ and from $7.29 \cdot 10^{-19}$ to $1.90 \cdot 10^{-17}$ $m^2/s$ for 0.15 M and 0.30 M $Ca(OH)_2$, respectively.
5. Rate of the process is dependent on suspension concentration (91.2% probability).
6. Value of the concentration-independent kinetic coefficient is $K_c = 2.8 \cdot 10^{-18}$ $m^2 \cdot M^{2/3}/s$. Modified GB model, which takes into account calcium hydroxide concentration, is the following

$$1 - \frac{2}{3}G - (1-G)^{\frac{2}{3}} = \frac{K_c \tau}{C_{Ca(OH)_2}^{\frac{2}{3}} R^2}.$$

# Acknowledgements

The first author (Andrey) is thankful to doc. Ilo Dreyer and Imants Kreicbergs for their support and supervision during the work on bachelor thesis back in 2014, which this study is based on. Andrey is especially thankful to his beloved Oksana V. Golubova.


# References


[1] AFSHAR A., GHORBANI M., EHSANI N., SAERI M.R., SORRELL C.C., *Some important factors in the wet precipitation process of hydroxyapatite*, Mater. Des., 2003, 24(3), 197–202.

[2] BĒRZIŅA-CIMDIŅA L., DREIJERS I., KREICBERGS I., *Hypothesis of $Ca(OH)_2$ and $H_3PO_4$ reaction mechanism on solid particle surface*, International Forum of Young Researchers "Topical Issues of Subsoil Usage", St. Petersburg, Russia, Apr. 20–22, 2011.

[3] BLANTON T.N., BARNES C.L., *D-75 Quantitative analysis of calcium oxide desiccant conversion to calcium hydroxide using X-ray diffraction*, Powder Diffr., 2004, 19(2), 45–51.

[4] BRUNDAVANAM R.K., POINERN G.E.J., FAWCETT D., *Modelling the crystal structure of a 30 nm sized particle based hydroxyapatite powder synthesised under the influence of ultrasound irradiation from X-ray powder diffraction data*, Am. J. Mater. Sci., 2013, 3(4), 84–90.

[5] GAO P., WANG H., JIN Z., *Study of oxidation properties and decomposition kinetics of three-dimensional (3-D) braided carbon fiber*, Thermochim. Acta, 2004, 414(1), 59–63.

[6] GINSTLING A.M, BROUNSHTEIN B.I., *О диффузионной кинетике реакций в сферических частицах*, Журнал прикладной химии, 1950, 23(12), 1249–1259 (in Russian).

[7] HENCH L.L., JONES J.R., *Biomaterials, artificial organs and tissue engineering*, 1st ed., Woodhead Publishing, Cambridge, 2005.

[8] HOU C.H., HOU S.M., HSUEH Y.S., LIN J., WU H.C., LIN F.H., *The in vivo performance of biomagnetic hydroxyapatite nanoparticles in cancer hyperthermia therapy*, Biomaterials, 2009, 30(23–24), 3956–3960.

[9] JAIN A., JOSEPH K., ANTHONYSAMY S., GUPTA G.S., *Kinetics of oxidation of boron powder*, Thermochim. Acta, 2011, 514(1–2), 67–73.

[10] KHACHANI M., EL HAMIDI A., KACIMI M., HALIM M., ARSALANE S., *Kinetic approach of multi-step thermal decomposition processes of iron(III) phosphate dihydrate $FePO_4{\cdot}2H_2O$*, Thermochim. Acta, 2015, 610, 29–36.

[11] KIM D.W., CHO I.-S., KIM J.Y., JANG H.L., HAN G.S., RYU H.-S., SHIN H., JUNG. H.S., KIM H., HONG K.S., *Simple large-scale synthesis of hydroxyapatite nanoparticles: in situ observation of crystallization process*, Langmuir, 2009, 26(1), 384–388.

[12] KRAUKLIS A.E., DREYER I., *A Simplistic Preliminary Assessment of Ginstling–Brounshtein Model for Solid Spherical Particles in the Context of a Diffusion-Controlled Synthesis*, Open Chem., 2018, 16(1), 64–72.

[13] MESKI S., ZIANI S., KHIREDDINE H., *Removal of lead ions by hydroxyapatite prepared from the egg shell*, J. Chem. Eng. Data, 2010, 55(9), 3923–3928.

[14] OZOLA R., KRAUKLIS A., BURLAKOVS J., VINCEVICA-GAILE Z., RUDOVICA V., TRUBACA-BOGINSKA A., BOROVIKOVA D., BHATNAGAR A., VIRCAVA I., KLAVINS M., *Illite clay modified with hydroxyapatite – innovative perspectives for soil remediation from lead (II)*, Int. J. Agric. Environ. Res. (IJAER), 2017, 3(2), 177–189.

[15] PTÁČEK P., NOSKOVÁ M., BRANDŠTETR J., ŠOUKAL F., OPRAVIL T., *Mechanism and kinetics of wollastonite fibre dissolution in the aqueous solution of acetic acid*, Powder Technol., 2011, 206(3), 338–344.

[16] QIFENG S., JIAYUN Z., BAIJUN Y., JIANHUA L., *Phase formation mechanism and kinetics in solid-state synthesis of undoped and calcium-doped lanthanum manganite*, Mater. Res. Bull., 2009, 44(3), 649–653.

[17] SADAT-SHOJAI M., KHORASANI M.-T., DINPANAH--KHOSHDARGI E., JAMSHIDI A., *Synthesis methods for nanosized hydroxyapatite with diverse structures*, Acta Biomater., 2013, 9(8), 7591–7621.

[18] SHAOXIAN Z., ZHIXIONG Y., PING L., GUANGHONG X., WANPENG C., *Hydroxyapatite/$Al_2O_3$ composite biomaterial implant*, Mater. Res. Soc. Symp. Proc., 1992, 292.

[19] SOKOLOVA M., PUTNIŅŠ A., KREICBERGS I., *The impact of mixing and $Ca(OH)_2$ suspension concentration on hydroxyapatite synthesis*, Riga Technical University 53rd International Scientific Conference, Riga, Latvia, Oct. 10–12, 2012, RTU Alumni: Digest, Riga, 2012.

[20] SOUNDRAPANDIAN C., BHARATI S., BASU D., DATTA S., *Studies on novel bioactive glasses and bioactive glass-nano-HAp composites suitable for coating on metallic implants*. Ceram. Int., 2011, 37(3), 759–769.

[21] TUDORACHI N., MUSTATA F., *Curing and thermal degradation of diglycidyl ether of bisphenol A epoxy resin crosslinked with natural hydroxy acids as environmentally friendly hardeners*, Arabian J. Chem., (in press), DOI: 10.1016/j.arabjc.2017.07.008.

[22] VALLET-REGÍ M., GONZÁLES-CALBET J.M., *Calcium phosphates as substitution of bone tissues*, Prog. Solid State Chem., 2004, 32(1–2), 1–31.

[23] VISWANATH B., RAVISHANKAR N., *Controlled synthesis of plate-shaped hydroxyapatite and implications for the morphology of the apatite phase in bone*, Biomaterials, 2008, 29(36), 4855–4863.

[24] WIONCZYK B., APOSTOLUK W., CHAREWICZ W.A., ADAMSKI Z., *Recovery of chromium(III) from wastes of uncolored chromium leathers*. Part I. *Kinetic studies on alkaline hydrolytic decomposition of the wastes*, Sep. Purif. Technol., 2011, 81(2), 223–236.

[25] ZAHOUILY M., ABROUKI Y., BAHLAOUAN B., RAYADH A., SEBTI S., *Hydroxyapatite: new efficient catalyst for the Michael addition*, Catal. Commun., 2003, 4(10), 521–524.